





Article

Design and Implementation of a Low-Cost and Low-Power Converter to Drive a Single-Phase Motor

Hudson V. Coutinho ¹, Jose A. Toledo ¹, Leonardo A. R. Silva ² and Thales A. C. Maia ^{3,*}

¹ Graduate Program in Electrical Engineering, Universidade Federal de Minas Gerais, Av. Antônio Carlos 6627, Belo Horizonte 31270-901, MG, Brazil; huvico@ufmg.br (H.V.C.); jtoledo@ufmg.br (J.A.T.)

² Department of Telecommunications and Mechatronics Engineering, Universidade Federal de São João del-Rei, Rod. MG 443 Km 7, Ouro Branco 36420-000, MG, Brazil; leonardo@ufsj.edu.br

³ Department of Electrical Engineering, Universidade Federal de Minas Gerais, Av. Antônio Carlos 6627, Belo Horizonte 31270-901, MG, Brazil

* Correspondence: thales@ufmg.br

Abstract: This research introduces a cost-effective converter for single-phase machines, aiming to enhance efficiency and reduce energy consumption in retrofit applications. Single-phase motors commonly found in household appliances often suffer from low efficiency, resulting in wasted energy. To tackle this problem, a dedicated converter was proposed to replace the existing capacitors and improve the motor performance. This study presents a proof of concept for retrofit applications, discussing the converter design methodology and prototype evaluation. Additionally, a cost analysis comparing single-phase and three-phase motors is included. It aims to demonstrate the long-term cost savings and improved energy efficiency of the proposed converter. The findings highlight the converter's potential as a promising solution for enhancing energy efficiency and decreasing costs in single-phase motor applications.

Keywords: efficiency; household appliances; low-cost converter; market survey; single-phase induction motor; power electronics; micro-power module



Citation: Coutinho, H.V.; Toledo, J.A.; Silva, L.A.R.; Maia, T.A.C. Design and Implementation of a Low-Cost and Low-Power Converter to Drive a Single-Phase Motor. *Machines* **2023**, *11*, 673. <https://doi.org/10.3390/machines11070673>

Academic Editors: Loránd Szabó and Feng Chai

Received: 4 May 2023

Revised: 11 June 2023

Accepted: 19 June 2023

Published: 21 June 2023



Copyright: © 2023 by the authors. Licensee MDPI, Basel, Switzerland. This article is an open access article distributed under the terms and conditions of the Creative Commons Attribution (CC BY) license (<https://creativecommons.org/licenses/by/4.0/>).

1. Introduction

Fossil fuels represent the primary source of energy worldwide, accounting for approximately two-thirds of global energy production [1]. The consumption rates of these fuels have been steadily increasing, particularly in countries experiencing industrial and demographic expansion, with annual growth rates ranging from 1% to 2% [2]. Nevertheless, this surge in demand has resulted in a corresponding escalation in CO₂ emissions [3], intensifying global apprehensions regarding climate change and prompting renewed endeavors to enhance energy efficiency, including that of electric motors.

Electric motors play a crucial role in global energy demand, accounting for approximately 40% of energy consumption [4]. Among various types of motors, single-phase motors represent approximately 9% of industrial demand [5] and nearly half of residential electric consumption [6,7]. They are commonly used in appliances such as washing machines, refrigerators, and air conditioners, as well as in air compressors, pumping systems, and other types of machinery [5,8]. However, their efficiency and torque ripple are compromised at a low load due to load variation [9].

Single-phase motors suffer from a low starting torque and low efficiency, resulting in significant energy waste. Even motors with 1 horsepower or more exhibit an efficiency of only 78% [10]. As a result, in many instances, single-phase motors are oversized in order to meet the high starting torque requirements, leading to low-load operation and a reduced efficiency. Therefore, enhancing the efficiency of these applications is critical in order to reduce energy consumption.

The utilization of frequency inverters and innovative control methods has the potential to significantly enhance performance and reduce losses [11]. By adopting this technology, energy consumption can be reduced by up to 30%. Studies have demonstrated that air conditioners can achieve efficiencies of up to 51.7% depending on the duty cycle and climatic conditions [12,13]. However, it is important to note that this solution is more suitable for new equipment that employs three-phase permanent magnet motors and may not be financially feasible for retrofit applications utilizing single-phase motors.

According to the literature, employing a frequency inverter with rotation measurement can lead to a significant reduction in energy consumption, such as up to 43% with a single-phase motor [14]. However, the incorporation of a rotation sensor may increase costs, and the availability of symmetrical coils can be limited. To address these challenges, a more versatile control approach has been proposed, capable of handling asymmetrical coils [15–17] and enabling sensorless control by estimating the motor's variables [18].

Replacing a single-phase motor with a three-phase motor may not be an attractive option for several reasons. Firstly, many existing single-phase motors are still in good operating condition [19]. Secondly, residential power supply is typically provided in a single phase, not in three phases. Therefore, utilizing a dedicated frequency inverter for driving a single-phase motor can be a viable alternative, provided that the cost of the converter is low, compatible with the power level, and offers a good performance.

With the continuous decline in the cost of semiconductors [20], the development of inexpensive and specialized converters to enhance the energy efficiency and performance of single-phase motors is becoming increasingly feasible. These converters have the potential to replace the capacitors commonly used with single-phase motors as they contribute to the overall cost without providing substantial improvements. By adopting these new converters, significant advancements can be made in terms of cost-effectiveness and energy savings, leading to even greater benefits.

This paper presents a design methodology for a low-cost and low-power converter dedicated to driving single-phase motors, with the aim of improving the efficiency of household appliances. The research includes a simulation and experimental validation of the prototype on a test bench, as well as a market survey to evaluate the feasibility of the proposed converter in comparison to the price difference between single-phase and three-phase motors. The primary focus of the work is to provide a technological proof of concept with a specific emphasis on retrofit applications, while also presenting the methodology for converter development.

2. Problem Statement and Relevance

Single-phase induction motors are extensively utilized in low-power applications, representing nearly 90% of all electric motors in the global stock, with an estimated 2 billion motors rated up to 750 W [21]. These motors are commonly found in various household appliances, including refrigerators, air conditioners, washing machines, dryers, microwaves, heat pump systems, and hydraulic pumping equipment. In rural areas, where consumers bear the cost of electrification, the supply of electricity is typically limited to single-phase power, making these motors indispensable for irrigation and artesian well systems.

Single-phase motors are favored not only for their compatibility with household appliances [6,7] but also due to their cost-effectiveness compared to three-phase motors. However, single-phase motors have inherent limitations in terms of efficiency and are susceptible to high torque ripple as a result of their operating principle [9].

2.1. Motors Benchmarking

To evaluate the economic feasibility, a simplified price analysis of single-phase and three-phase motors based on the Brazilian market is presented. The objective was to assess the power range suitable for a single-phase converter. For this market survey, Figure 1 shows the prices of 161 motors with 4 poles and power ranging from 1/4 to 10 hp, among 4 different brands. It is important to note that there is a significant price

variation due to various motor classifications based on the degree of internal protection (IP). To obtain a median value from a homogeneous set, the IP classification was not considered in this analysis.

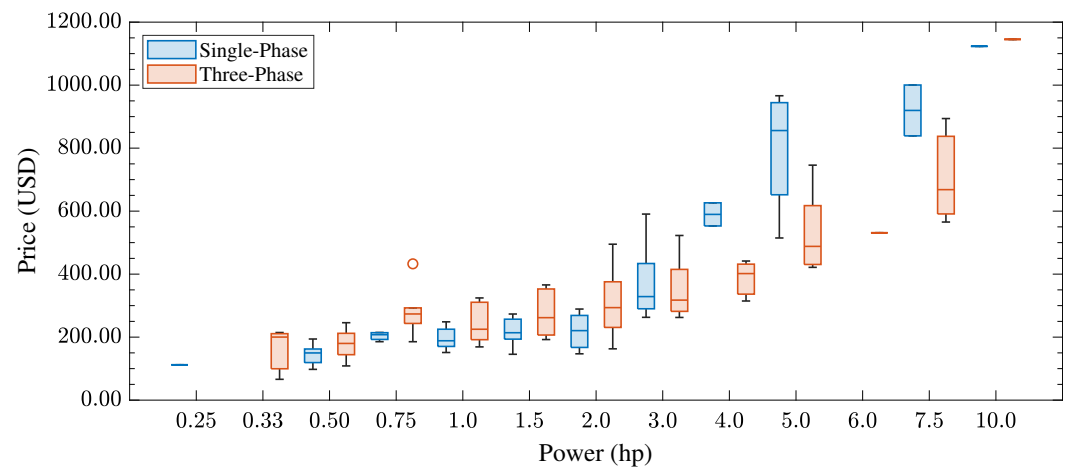


Figure 1. Comparative study of prices of single- and three-phase four-pole motors for different powers, computed on 12 October 2022.

Figure 2a shows the median prices for each shaft power and for each motor type, whereas Figure 2b shows the price difference between both motors type for some shaft power. It is noteworthy that, for low power ratings up to 2 hp, the single-phase motor is more affordable than the three-phase motor, thus reinforcing the notion that single-phase motors remain economically advantageous for such applications.

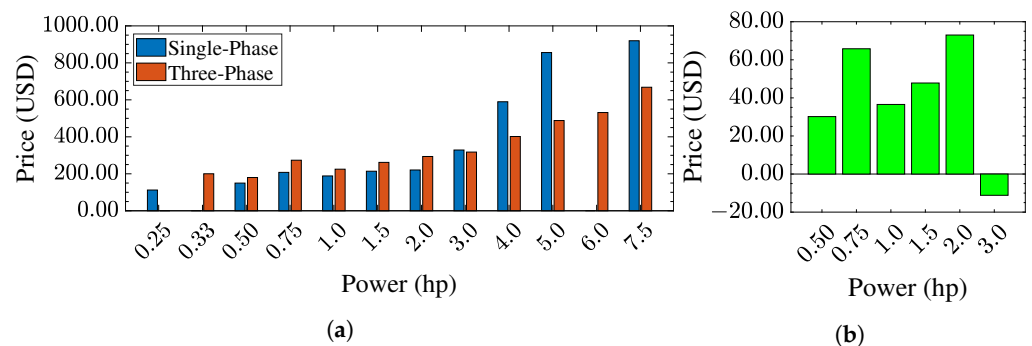


Figure 2. Price comparison between the power of four-pole single- and three-phase motors. (a) Median price. (b) Price difference.

It is worth noting that, even in households with access to a three-phase power supply, which represent a minority, the addition of a cheap converter is justified by the price difference between low-power single-phase and three-phase motors. It is more advantageous to drive a single-phase motor using the converter compared to directly starting a three-phase motor. For instance, in the case of a 1 hp motor, converters priced up to USD 37.00 become financially appealing.

It is important to emphasize that the market survey presented solely considers the equipment acquisition cost and does not account for the operating cost, which is ultimately borne by the consumer. However, when considering the efficiency gains and potential energy savings, the overall return on investment is expected to be even more favorable.

2.2. Motor and Converter Technologies

To operate a single-phase motor using the voltage grid, a capacitor is required to induce a phase-shift in the current, enabling the generation of a rotating magnetic field [22]. However, variations in the capacitor's aged value can cause cogging torque, thereby

reducing the motor's efficiency even under rated load conditions. Furthermore, the motor may experience efficiency losses if the load falls below its rated value.

In typical scenarios, single-phase motors are directly powered by the mains voltage. However, achieving speed control necessitates voltage variation through the use of a rheostat, which is inefficient and reduces the available torque. To enhance efficiency and drive flexibility, static converters can be employed. These converters allow for speed and torque variation in the motor through control strategies aimed at optimizing efficiency or maximizing torque [14,23,24].

The three most commonly used converter topologies for driving single-phase motors are the dual half-bridge, three half-bridge, and dual full-bridge configurations [25]. By employing a space vector pulse width modulation (SVPWM) technique, the converter can generate voltage space vectors within the regions depicted in Figure 3. These regions encompass the range of desired voltage V^* that can be synthesized by the converter, which differs from the three-phase case.

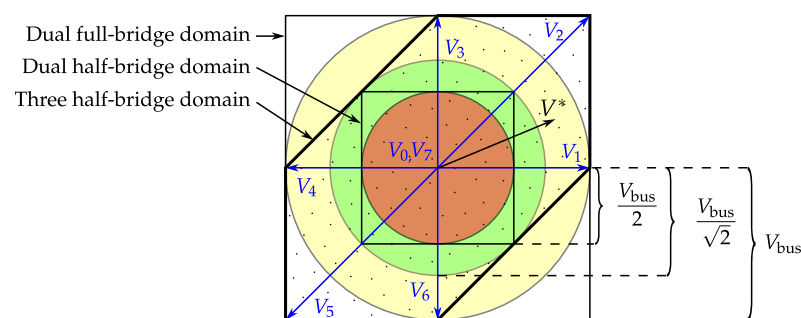


Figure 3. Illustrative drawing of three different domains applied to the single-phase converter.

In the case of the three half-bridge topology, there are eight possible switching combinations that result in voltages V_0 to V_7 . By appropriately sequencing these voltages during the switching period, the desired voltage can be achieved. To maintain a constant motor torque, the voltage V^* should remain within the domain circle. For instance, with the three half-bridge converter, it is capable of synthesizing any voltage within the shaded region. However, to ensure constant torque, the voltage should not exceed the limit defined by the green circle.

The dual half-bridge topology is a cost-effective option as it utilizes only four switches. It employs a DC voltage bus with two capacitors that create a central neutral point, which is connected to the winding's neutral point. However, this topology has the drawback of providing a low output voltage magnitude of $V_{bus}/2$ (represented by the red circle in Figure 3) and is unable to generate a zero-voltage vector. Additionally, to achieve symmetrical voltages, the capacitors must be identical, which can be challenging due to the different physical characteristics of the auxiliary and main motor windings. This results in asymmetric currents flowing through the capacitors and leads to different voltages across each capacitor. Therefore, compensation techniques are necessary in the switching control to address this issue [18].

Another topology option is to use a full-bridge configuration for each winding, which requires eight switches. Although this topology is more expensive compared to others, it effectively utilizes the DC bus voltage and generates a first-order output voltage magnitude of V_{bus} (represented by the yellow circle in Figure 3). Furthermore, each coil is fed independently, resulting in an uncoupled system. This topology has been studied in various works, such as [26,27]. Additionally, an elliptical SVPWM technique has been proposed to generate any unbalanced two-phase output voltage for feeding an asymmetrical bi-phase induction motor. This technique helps to reduce pulsations in electromagnetic torque, leading to an improved speed control [28].

In this paper, the most commonly used topology, shown in Figure 4, was employed. This topology utilizes three half-bridges with six switches to achieve an output voltage

magnitude of $V_{bus}/\sqrt{2}$ (represented by the green circle in Figure 3) [29]. This topology has been widely studied and applied in various academic papers, including those focused on field-oriented control strategies [14], direct torque control in symmetrical two-phase motors [30], rotor-flux-oriented control considering asymmetric coils and torque cogging elimination [18] (without cost and efficiency analysis), and slip frequency control with constant V/f using a feedback encoder [31].

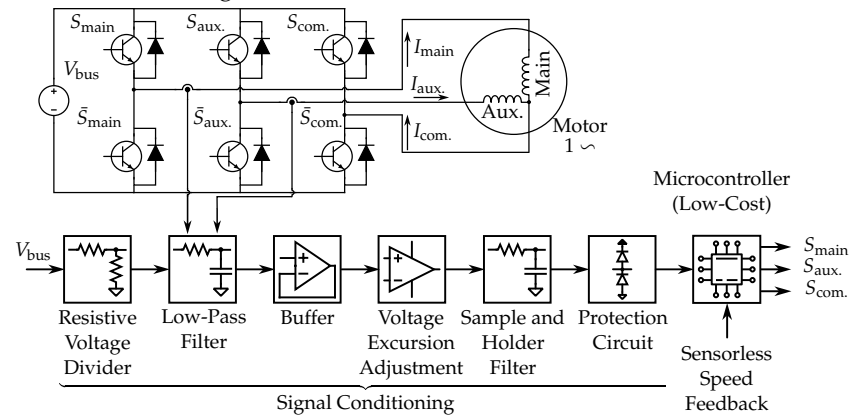


Figure 4. Illustrative schematic of the power converter components that are integrated to drive a single-phase motor.

It is worth noting that, in the presented topology, the common leg functions as a virtual neutral point and carries a higher current compared to the other legs due to the summation of the two currents [28]. This characteristic should be taken into consideration when sizing the electronic switches to ensure that they can handle the required current. Furthermore, power modules integrated with the six switches are widely available, enabling the design of a compact and simplified converter, which adds to the attractiveness of this topology for converter design.

3. Methodology

When designing a converter, it is necessary to determine the voltage and current requirements in order to calculate the rated output and input power, as well as the switching frequency and operation mode. The specification of components is based on factors such as voltage drop, thermal behavior, and impedance. The design methodology is an interactive process, as illustrated in Figure 5, that involves iterative checks on operating parameters, transients, and thermal behavior to meet the cost target and ensure proper functionality.

The steps discussed earlier were evaluated in the specification of the converter topology. The schematic diagram shown in Figure 4 is divided into two sections: the power circuit and the signal circuit. The rectified voltage from the DC bus is supplied to the input of the three-phase IGBT integrated module, along with the six PWM signals that control the activation of the switches. Two output currents from the converter are measured using Hall effect sensors, and the corresponding voltage signals are conditioned and made available to the signal circuit. These voltage signals are then processed and prepared for use at the inputs of a microcontroller, along with the measurement of the DC bus voltage. The microcontroller performs signal processing and generates the PWM signals to control the electronic switches.

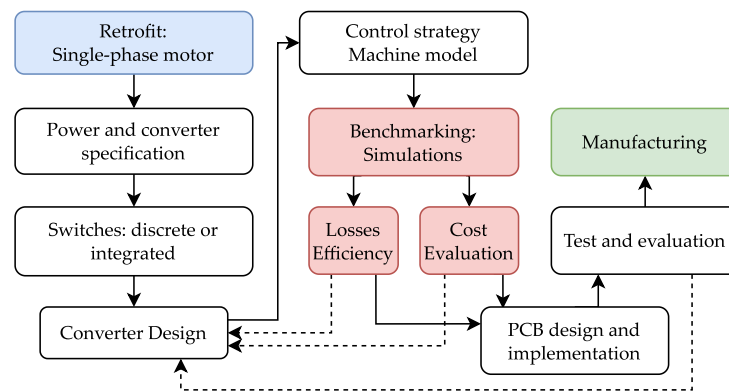


Figure 5. The main steps of the converter design methodology for achieving a satisfactory design result for manufacturing.

4. Converter Design

In this work, the objective was to design a cost-effective converter that fulfills the specific requirements outlined in Table 1. The converter is intended to be used for powering low-power household appliances. To achieve this objective, the converter design was optimized to minimize costs while ensuring that all the necessary requirements were met.

Table 1. Requirements for the converter design.

Group	Requirement
Cost	Meets the Low-Cost Features
Specifications	Works on a mains voltage up to 220 Vac/60 Hz Feeds a load of up to 1 hp
Switches	Integrated three-phase IGBT module with heat sink
Sensors	Measures two output currents with Hall sensors Measures the voltage bus with a resistive divider
Control	Conditions the output signals to microcontrollers Maximum switching of 5 kHz

4.1. Specification of the DC Bus Components and IGBT Module

Indeed, the DC bus plays a crucial role in power electronics systems, and its design should not be overlooked. To address issues such as total harmonic distortion (THD) and power factor improvement, more advanced filtering techniques can be employed. These filters help to reduce harmonics and improve the overall quality of the input power waveform [32]. Additionally, at higher power levels, the presence of leakage inductance between the grid and the rectifier input can result in significant voltage drops. It is important to consider these factors during the design process to ensure the proper functioning and efficiency of the converter.

The choice of an integrated diode rectifier bridge for converting the 127–220 AC voltage into DC voltage is a common and practical solution. The specified current rating of 25 A at 60 Hz indicates the capability of the rectifier bridge to handle the expected current requirements of the load, which, in this case, corresponds to a load of 1 hp.

When designing the filter, the cost of the capacitor is an important consideration. Research has shown that the cost of a capacitor is directly proportional to its volume [33]. Additionally, the rated voltage of the capacitor also affects its volume. Consequently, a converter designed to operate at a lower DC bus voltage will require a smaller and more affordable capacitor compared to a higher voltage level. In this case, an electrolytic capacitor with a voltage rating of 450 V was selected, taking into account its availability and affordability.

An integrated module with IGBTs was chosen for the converter design due to its suitability for household appliances, cost-effectiveness, and compact size. The selected module features three half-bridge IGBTs with reverse conduction capability provided by a monolithic diode. It is rated for a maximum current of 20 A, which meets the requirements for driving low-power household appliances. By utilizing this integrated module, the design achieves the desired functionality while optimizing space utilization and cost efficiency.

4.2. Specification of the Heat Sink

Proper thermal calculation is crucial for designing the heat sink of static switches and evaluating the thermal conditions during operation to prevent semiconductor failure and damage. It is important to note that the maximum output power in a steady state is determined by the switching frequency and output current of the converter.

Estimating the junction temperature of the devices can be accomplished by modeling the current and voltage transients in the switches and analyzing the thermal effects during overload pulses. However, the calculation can be simplified by focusing on steady-state conditions, which provide a good approximation of the device's thermal behavior [34].

The designed converter model underwent simulation to obtain the current and voltage values in each IGBT for the steady-state condition, as well as the switching times. The total losses were calculated using the IGBT parameters provided in the datasheet. To model the thermal conditions in the steady state, a thermal circuit, as shown in Figure 6, was employed [35,36]. Subsequent simulations were conducted to determine the required thermal resistance of the heat sink in order to maintain the junction temperature within a safe limit of 140 °C, as depicted in Figure 7.

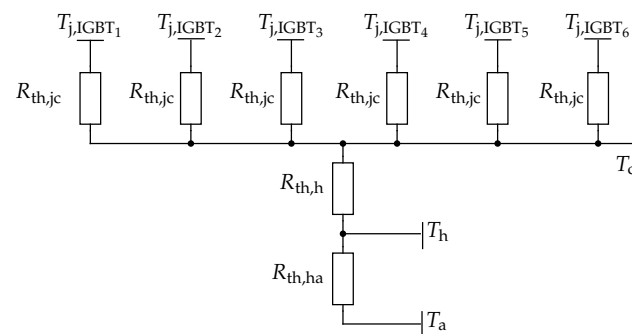


Figure 6. Simplified thermal equivalent circuit applied to the thermal analysis.

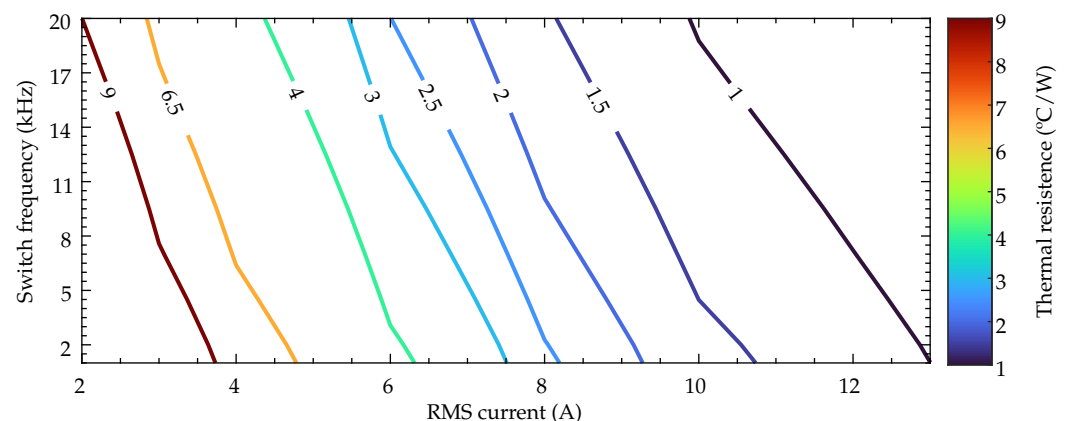


Figure 7. Maximum thermal resistance depending on switching frequency and output current.

Based on the results presented in Figure 7, a heat sink with dimensions of $56 \times 30 \times 20$ mm and a thermal resistance of $5.33 \text{ }^\circ\text{C/W}$ was selected. Subsequent simulations were conducted to observe the junction temperature in the steady state as a function of output current and switching frequency, considering the chosen heat sink. The results are illus-

trated in Figure 8. It should be noted that using a fan in conjunction with the heat sink can reduce the equivalent thermal resistance and enhance thermal exchange with the environment, thereby allowing for a higher output current. However, increasing the switching frequency reduces the maximum current that the converter can sustain.

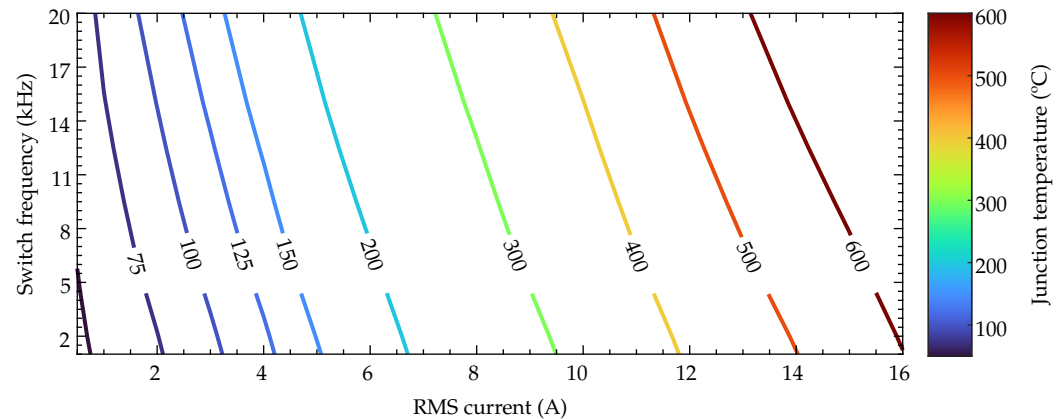


Figure 8. Maximum junction temperature depending on switching frequency and output current.

4.3. Specification of the DC Bus and Output Current Signals Conditioning Circuit

The circuit schematics are depicted in Figure 9. To condition the voltage, a resistive voltage divider was employed, followed by a low-pass filter to filter out any high-frequency components. The resulting signal was then buffered and fine-tuned by the excursion adjustment circuit. Subsequently, the processed output voltage was fed into the microcontroller for further processing. The circuit diagram specifically designed for voltage measurement is shown in Figure 9a.

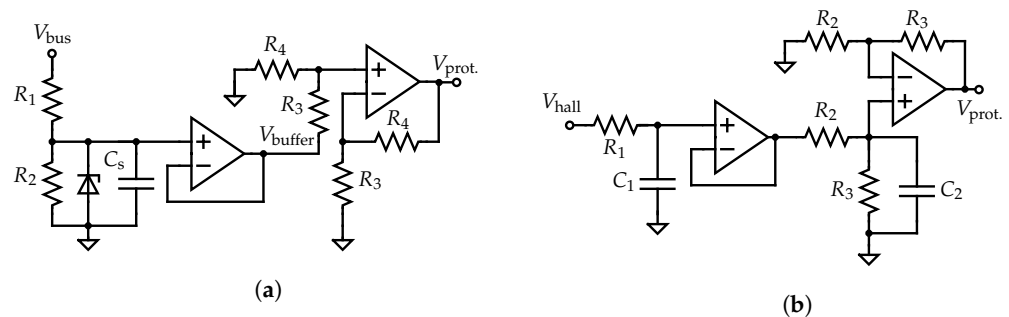


Figure 9. Schematic of a voltage and current signal conditioner circuit to measure the DC bus voltage and the main and auxiliary winding currents. (a) Voltage conditioner. (b) Current conditioner.

To ensure the reliability and prevent excessive voltage-related failures of the surface mount device (SMD)-type resistors, the resistive divider R_1 was constructed using resistors connected in series. This arrangement effectively reduces the voltage across the terminals of each resistor. Furthermore, a capacitor was incorporated into the resistive divider to filter out high-frequency components and minimize noise above the cut-off frequency. To provide additional protection against voltage surges, a Zener diode was included in the circuit. This diode acts as a voltage clamp, limiting the maximum voltage that can be applied to the circuit and offering an extra layer of safeguarding.

The system utilizes Hall effect transducers to measure two of the output currents, whereas the third current is estimated by summing the other two measurements. One notable advantage of these transducers is their ability to provide electrical isolation between the measured circuit and their output. This feature eliminates concerns related to common-mode voltage and enhances the accuracy and reliability of the current measurements.

As depicted in Figure 9b, the transducer voltage V_{hall} first undergoes low-pass filtering before being buffered. Subsequently, the buffered voltage is adjusted by the voltage excursion adjustment circuit to ensure accurate measurement within the desired range.

The resulting output voltage is then accessible to the microcontroller for further processing, similar to the bus voltage measurement described earlier.

4.4. Specification of the Protection Circuit and Auxiliary Voltage Sources

To safeguard the microcontroller pins and prevent damage, a protection circuit with a diode clamper was incorporated. This circuit limits the voltage levels applied to the microcontroller, preventing potential overvoltage situations. Furthermore, a sample-and-hold capacitor was integrated into the circuit design to minimize any signal interference and provide stable voltage levels during sampling.

In order to provide the necessary auxiliary voltage to power both modules and microcontrollers, an AC/DC converter module was employed. By utilizing pre-designed modules, the design time and costs associated with developing a custom power supply circuit were significantly reduced. This makes the use of modules an attractive option, allowing for a streamlined and cost-effective implementation in this application.

4.5. Design of the Control Loop

To minimize torque pulsation in single-phase motors, it is crucial to implement a control strategy that specifically addresses motor asymmetry. One effective approach is rotor flux-oriented control, which involves a mathematically derived treatment of motor currents. The references [18,37] provide detailed insights and results regarding the implementation of this control strategy, enabling other researchers to further investigate and clarify the expected performance under various operating conditions. These references serve as valuable resources for understanding and optimizing the control loop for reducing torque pulsation in single-phase motors.

The torque produced by the motor depends on various factors, including the number of pole pairs (P), the rotor inductance (l_r), the mutual inductance (\mathcal{M}), the stator current (i_s), and the rotor flux (ϕ_r). The torque can be defined as follows:

$$T_e = \frac{P}{l_r} (\mathcal{M}_q i_{sq} \phi_{rd} - \mathcal{M}_d i_{sd} \phi_{rq}). \quad (1)$$

It is worth noting that the oscillatory term can be effectively compensated for by setting the ratio of the rotor flux components $|\phi_{rd}|/|\phi_{rq}| = 1$ and the ratio of the stator current components $|i_{sd}|/|i_{sq}| = \mathcal{M}_d/\mathcal{M}_q$. This compensation approach is based on the turns ratio (k) between the auxiliary and main windings and allows for the adjustment of current amplitudes.

For the purpose of this study, the introduction of auxiliary currents i_{sd1} and i_{sq1} , as well as the correction factor $k = \mathcal{M}_d/\mathcal{M}_q$, allows for addressing the asymmetry in the motor system. By assuming that the imposed motor currents are given by $i_{sd} = i_{sd1}$ and $i_{sq} = k \cdot i_{sq1}$, we can substitute them into Equation (1) to obtain an equivalent torque equation that resembles a symmetrical motor system. The resulting equation

$$T_e = \frac{P}{l_r} \mathcal{M}_d (i_{sq1} \phi_{rd} - i_{sd1} \phi_{rq}) \quad (2)$$

eliminates torque pulsation and yields a rotor behavior that is similar to that of a three-phase machine referenced on the dq axis.

This control strategy for a motor system utilizing field orientation of the rotor flux was simulated. In this method, the control input references are the motor torque and flux. The direct and quadrature motor currents were subsequently calculated and imposed by the converter, as illustrated in Figure 10.

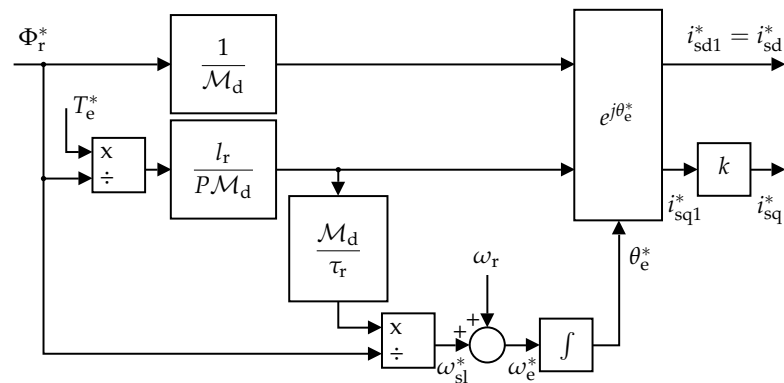


Figure 10. Block diagram of the field-oriented controller used in closed-loop torque control in an asymmetric single-phase motor.

This strategy was simulated to evaluate the efficiency map by considering a symmetrical and an asymmetrical motor (Figure 11a), as well as a capacitor-start motor (Figure 11b), including converter losses. The results are presented in Figure 11c. It is observed that there is an efficiency gain of up to 10%, depending on the load driven, when comparing a capacitor-driven motor and a control-loop-driven motor, considering both symmetric and asymmetric motor configurations. Additionally, it is noted that the symmetric motor outperforms the asymmetric motor in terms of efficiency across the entire power range.

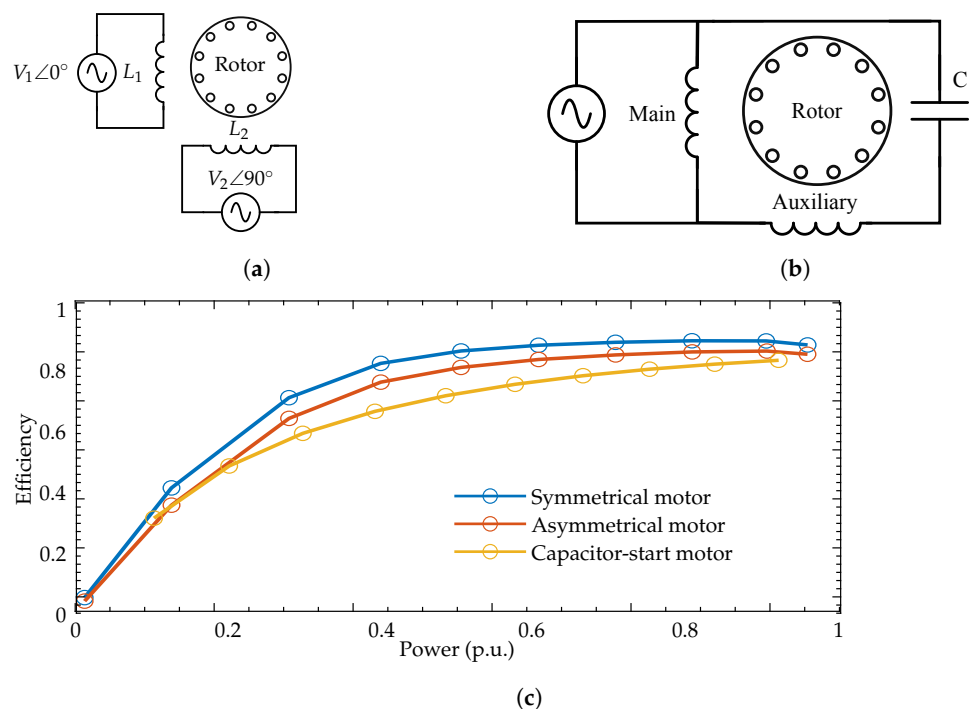


Figure 11. Comparison of the performance between an auxiliary capacitor drive and an inverter in function of the shaft load. (a) Symmetric and asymmetric motor. (b) Capacitor-start motor. (c) Motors efficiency map.

5. Experimental Results

The implemented converter, with a volume-to-power ratio of $660 \text{ mm}^3/\text{W}$, was used for the experimental tests shown in Figure 12. The test setup includes a 1 hp, 127 Vac, 2-pole single-phase induction machine manufactured by Eletroplas, a hydraulic pump, a LaunchPad from Texas Instruments with a TMS320F28379D processor, a multimeter for current and voltage measurement, a personal computer with Code Composer Studio, and an oscilloscope Hantek, model 6022bl.

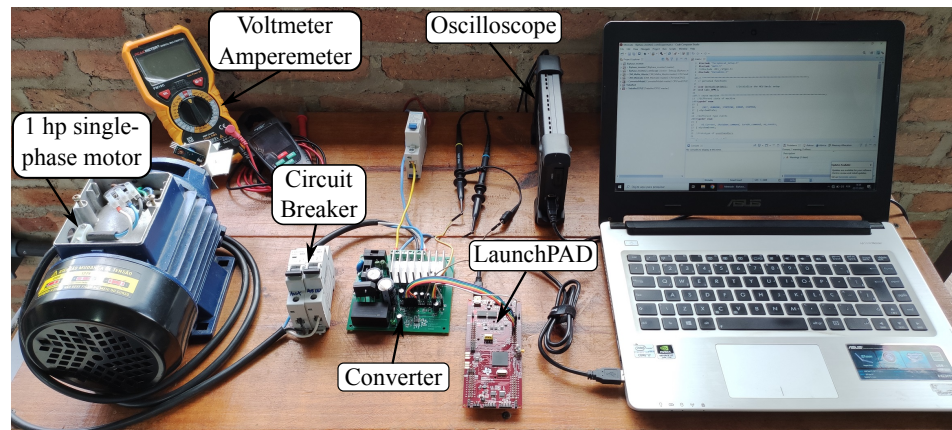


Figure 12. Complete setup used to collect the experimental results.

Initially, the motor was directly connected to the grid using its auxiliary capacitor, which drove the hydraulic pump coupled to its shaft. The steady-state grid voltage and current, as well as the auxiliary and main winding currents, are plotted in Figure 13. It was observed that the current distortion, caused by magnetic saturation, resulted in a significant THD in both the motor and grid currents. Table 2 presents the third, fifth, and seventh harmonic orders relative to the fundamental, as well as the calculated total THD.

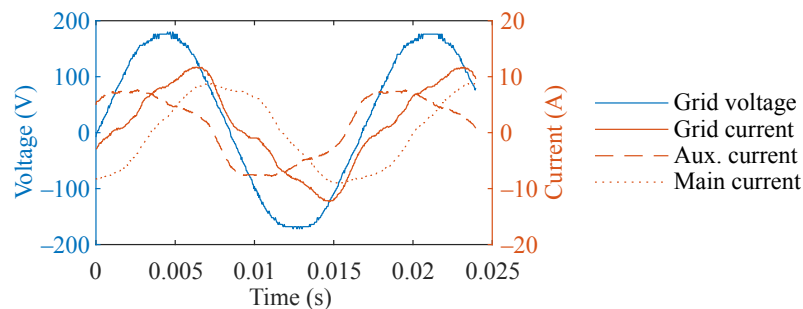


Figure 13. Grid voltage and current and auxiliary and main winding currents in a direct start using the auxiliary capacitor.

Table 2. Current magnitude of third, fifth, and seventh harmonic orders relative to the fundamental and total THD from main and auxiliary windings with rated load.

Order	With Inverter		Direct Start		
	Main	Aux	Main	Aux	Grid
3	14.73%	15.52%	4.95%	16.40%	15.27%
5	4.26%	4.06%	4.94%	7.79%	10.10%
7	1.22%	2.18%	0.94%	1.97%	0.65%
THD	16.06%	20.82%	7.30%	18.39	18.48%

Magnetic core saturation is often attributed to various factors, including the use of low-quality magnetic materials, inadequate design or operational conditions, and the presence of non-linear loads. These factors contribute to the saturation of the magnetic flux, resulting in increased core losses and a diminished magnetic performance. Consequently, the motor tends to draw a higher current than required.

Subsequently, the converter was connected to the 127 V/60 Hz grid source to operate the motor coupled with a hydraulic pump. In this experiment, an open-loop control strategy was employed with a 5 kHz PWM frequency for IGBT switching. The reference vector voltage was selected to follow a circular trajectory within the maximum allowable range, as depicted in Figure 3. The experimental outcomes, presented in Figure 14, display the main and auxiliary currents and voltages signals.

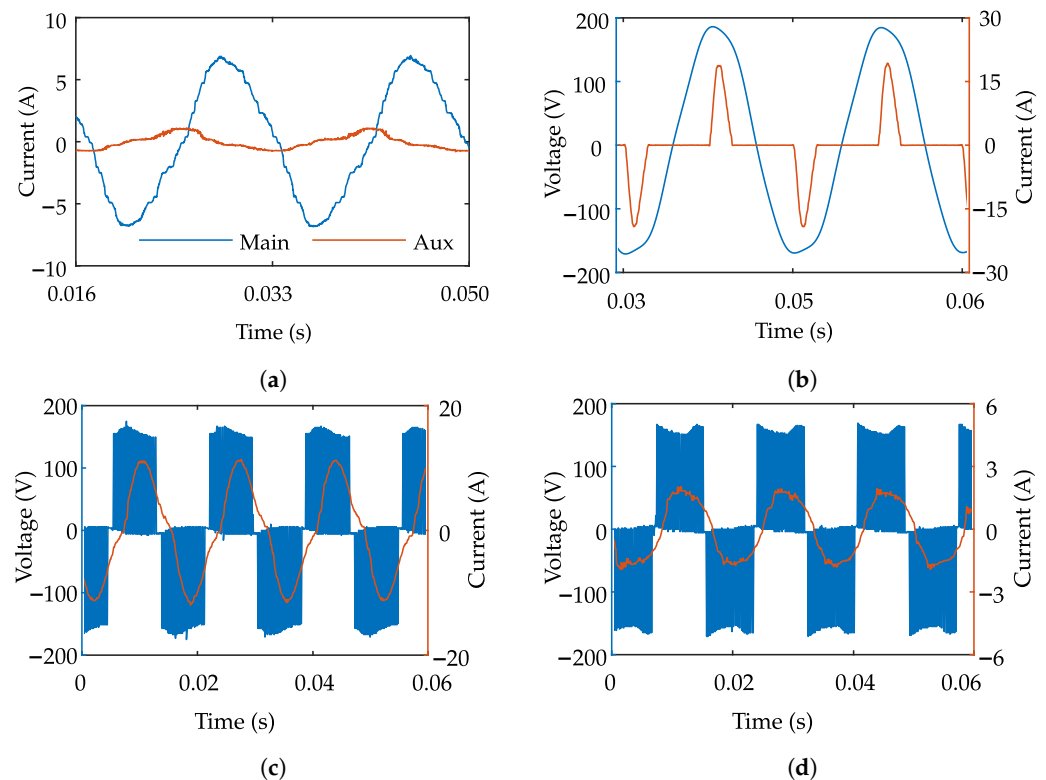


Figure 14. Current and voltage signals from converter driving the single-phase motor with a 5 kHz switching frequency. (a) Main and auxiliary currents, no load. (b) Grid voltage and current, full pump load. (c) Main voltage and current, full pump load. (d) Aux. voltage and current, full pump load.

Initially, the motor was started with no load, using an open-loop V/f constant ramp until it reached a steady state, as presented in Figure 14a. Subsequently, a load was added to the rotor shaft by fully opening the discharge valve of the pump, allowing for water circulation. The signals corresponding to the full pump load are depicted in Figure 14b–d. The line current waveform shown in Figure 14b is typical of a full bridge rectifier but suffers from high peaks of 20 A and high THD due to the proposed low-cost solution [38]. The current waveforms in Figure 14c,d exhibit distortion due to the poor quality of the motor’s magnetic material, as evidenced by the presence of third and fifth harmonics in Table 2.

The voltage fluctuations on the DC bus impose limitations on the achievable voltage vector domain and contribute to the harmonic content, creating a trade-off between THD and the utilization of the DC bus in the designed converter. To mitigate this distortion and improve the input current waveform toward a sine waveform, a DC voltage bus control method can be employed.

The current measurements also indicate the presence of high-frequency components, which are attributed to capacitive coupling between the measurement circuits and the PWM signals with high rates of the change in voltage (dV/dt) in the power circuits. These findings contribute valuable insights into the motor’s behavior and the effectiveness of the control strategy within the specific experimental conditions of this study.

The grid supplied an approximate power of 519 W, whereas the converter delivered 478 W to the motor, with 7.4 A to the main winding and 1.3 A to the auxiliary winding. The converter itself consumed around 40 W, resulting in an efficiency of approximately 92%. It is important to note that the power did not reach the rated level, potentially due to limitations imposed by the characteristic curve of the pump.

6. Converter Cost

The estimated total cost of the designed converter is USD 27.81, as calculated from the itemized costs listed in Table 3. This cost does not include the microcontroller and its power supply. The most expensive components in the converter include the IGBT module, the PCB with SMD components, the current sensors, the DC capacitors, the AC-DC 15 V module, and the 3 V regulator. It is important to focus on reducing the cost of these components to enhance the overall cost-effectiveness of the converter.

Table 3. Components cost of the implemented converter.

Description	Part Number	Quantity	Price (USD)	
			Unity	Total
IGBT Power Module	IGCM20F60GA	1	6.80	6.80
PCB with SMD components	-	1	5.87	5.87
Hall Effect Current Sensor	ACS712ELCTR-20A-T	2	1.44	2.88
Aluminum Electrolytic Capacitors	450 V 220 μ F	2	1.18	3.36
Power Modules AC-DC 15 V	TAS5-15-WEDT	1	2.80	2.80
Linear Voltage Regulators 3 V	TPS79730DCKT	1	2.19	2.19
Bridge Rectifiers	KBU2510	1	0.79	0.79
Aluminum Electrolytic Capacitors	35PX100MEFC6.3X11	10	0.06	0.63
Through-Hole Fuse Holders	FH1-200CK-B	2	0.29	0.57
Screw Terminal	JL500-50008GT1	1	0.51	0.51
Heat Sink	HS 5620	1	0.50	0.50
Diodes of General Purpose	BAS321,115	10	0.05	0.49
Unidirectional DO-201 TVS	1.5KE20A/B	2	0.19	0.38
Shunt Resistor 0.01 Ω (5 W)	-	2	0.18	0.37
Radial Leaded Varistors	STE14D431K1EN0FQB0R0	2	0.18	0.36
Operational Amplifier	LM358D	3	0.04	0.13
Unidirectional SOD-123F TVS	SMF5.0A	2	0.03	0.07
Aluminum Electrolytic Capacitors	KS226M035D07RR0VH2FP0	5	0.01	0.06
			27.81	

In an open-loop control application, it is indeed possible to eliminate the current sensors and the 3 V regulator, leading to cost savings of approximately USD 5.00 per converter. This demonstrates the significance of thoroughly evaluating the design requirements and selecting components that fulfill those requirements at the lowest feasible cost. By further optimizing the converter's design and selecting components judiciously, it is possible to achieve additional cost savings without compromising performance and reliability.

The estimated cost provided was based on the prototype design, and it is reasonable to expect a significant reduction in cost when scaling up to mass production. Mass production typically benefits from economies of scale, streamlined manufacturing processes, and the bulk purchasing of components, resulting in lower per-unit costs. Therefore, the proposed solution becomes even more attractive in terms of cost-effectiveness when produced in large quantities.

7. Conclusions

This paper presents the design process of an affordable converter specifically tailored for driving low-power single-phase motors commonly found in household appliances. Recognizing the limited availability of converters for such motors, the design stages were meticulously examined and refined to ensure cost reduction. Through simulation and experimental validation, a prototype was successfully developed, achieving an efficiency of 92%. This low-cost converter holds great potential as a viable solution for retrofit applications seeking efficiency enhancements.

In contrast to the conventional approach of utilizing a direct motor drive in appliances to avoid additional costs associated with power converters, this study showcases the feasibility of constructing a cost-effective converter for single-phase motors. Furthermore,

employing such a converter can result in operational efficiency improvements and potentially enable the downsizing of the motor thanks to better power utilization within the system. Consequently, the investment in the converter can be justified over time through energy savings or the use of a smaller and more economical motor.

The thermal analysis conducted during the design process played a vital role in determining the operational limitations of the converter. Despite the IGBT module having a rated current capacity of 20 A, the actual maximum current was constrained by the cooling effectiveness of the module. The design did not incorporate a fan, relying solely on a heat sink for thermal dissipation. However, by incorporating a fan along with the heat sink, the thermal design can be enhanced, enabling the converter to drive more powerful motors with increased efficiency and reliability.

The suboptimal quality of single-phase motors often leads to the occurrence of magnetic core saturation during their operation. This saturation phenomenon gives rise to the generation of significant harmonic components in both the grid current and motor current, consequently leading to a reduction in overall efficiency and the presence of torque pulsations. By employing higher-quality magnetic materials in the construction of single-phase motors, it is possible to enhance their efficiency. Furthermore, the implementation of advanced control techniques, such as field-oriented control, can effectively mitigate the adverse effects of harmonic distortion and torque pulsations, thereby improving the overall performance of the motor.

Future work will encompass several aspects to further enhance the understanding and performance of the single-phase motor drive. This includes developing a comprehensive model of the single-phase machine to accurately represent its torque and rotation control characteristics. Additionally, the implementation of a back-to-back assembly will be pursued to validate the control algorithms and investigate the energy efficiency of the drive utilizing the designed converter.

The planned research will involve studying the motor's performance under various operating conditions, including normal operation as well as critical scenarios such as sudden load changes, power supply variations, and speed fluctuations. Detailed analysis will be conducted to examine efficiency, torque output, and speed waveforms in each scenario, providing valuable insights into the drive's performance.

In addition, there are plans to develop and implement a control strategy for the DC bus voltage to regulate and stabilize its level. Furthermore, the closed-loop control approach mentioned in this paper for mitigating torque pulsation will be implemented on the microcontroller. The objective is to assess the effects of this control approach on even harmonics and their correlation with motor asymmetry. Through the study and optimization of the control strategy, it is anticipated that the overall performance and efficiency of the single-phase motor drive system can be further improved.

Author Contributions: Conceptualization, H.V.C., J.A.T., L.A.R.S. and T.A.C.M.; Methodology, H.V.C., J.A.T., L.A.R.S. and T.A.C.M.; Software, H.V.C.; Validation, H.V.C.; Investigation, H.V.C.; Writing—original draft, H.V.C.; Writing—review & editing, J.A.T. and L.A.R.S.; Supervision, T.A.C.M.; Project administration, T.A.C.M. All authors have read and agreed to the published version of the manuscript.

Funding: This research received no external funding.

Data Availability Statement: Data sharing not applicable.

Conflicts of Interest: The authors declare no conflict of interest.

References

1. Rivera-Durán, Y.; Berna-Escriche, C.; Córdova-Chávez, Y.; Muñoz-Cobo, J.L. Assessment of a Fully Renewable Generation System with Storage to Cost-Effectively Cover the Electricity Demand of Standalone Grids: The Case of the Canary Archipelago by 2040. *Machines* **2023**, *11*, 101. [CrossRef]
2. Ritchie, H.; Roser, M. Energy Production and Consumption: Our World in Data. 2022. Available online: <https://ourworldindata.org/energy-production-consumption> (accessed on 11 March 2022).

3. BP. *Statistical Review of World Energy*; Technical Report; BP: London, UK, 2022.
4. Tiwari, D.; Miscandlon, J.; Tiwari, A.; Jewell, G.W. A Review of Circular Economy Research for Electric Motors and the Role of Industry 4.0 Technologies. *Sustainability* **2021**, *13*, 9668. [\[CrossRef\]](#)
5. Sauer, I.L.; Tatizawa, H.; Salotti, F.A.; Mercedes, S.S. A Comparative Assessment of Brazilian Electric Motors Performance with Minimum Efficiency Standards. *Renew. Sustain. Energy Rev.* **2015**, *41*, 308–318. [\[CrossRef\]](#)
6. Abrahão, K.C.F.J.; Souza, R.G.V. Estimativa da evolução do uso final de energia elétrica no setor residencial do Brasil por região geográfica. *Ambiente Constr.* **2021**, *21*, 383–408. [\[CrossRef\]](#)
7. EPE. *Anuário Estatístico de Energia Elétrica 2020—Ano Base 2019*; Technical Report, Empresa de Pesquisa Energética (EPE): Brasília, Brazil, 2020.
8. de Rossiter Corrêa, M.B.; Jacobina, C.B.; Lima, A.M.N.; Silva, E.R.C. Motor Drive System For Single-phase Induction Motors—An Evaluation. *Eletrônica Potência* **2003**, *8*, 79–88. [\[CrossRef\]](#)
9. Um, D.Y.; Park, G.S. Comparison of Electromagnetic Characteristics of Single-Phase Induction Motor between Balanced and Unbalanced Operation under Different Loads. *Energies* **2021**, *14*, 919. [\[CrossRef\]](#)
10. Chasiotis, I.; Karnavas, Y.; Scuiller, F. Effect of Rotor Bars Shape on the Single-Phase Induction Motors Performance: An Analysis toward Their Efficiency Improvement. *Energies* **2022**, *15*, 717. [\[CrossRef\]](#)
11. Tan, D. Power Electronics: Historical Notes, Recent Advances and Contemporary Challenges. *Eletrônica Potência* **2020**, *25*, 386–394. [\[CrossRef\]](#)
12. Marangoni, F.; Tellini, T.; Moreno, R.P.R.; Ferreira, S.O.; Konopatzki, E.A. Comparativo Econômico entre Condicionadores de Ar com Tecnologias Convencional e Inverter. In Proceedings of the Encontro Nacional de Engenharia de Produção, Fortaleza, Brasil, 13–16 October 2015; p. 20.
13. Lim, J.; Yoon, M.S.; Al-Qahtani, T.; Nam, Y. Feasibility Study on Variable-Speed Air Conditioner under Hot Climate Based on Real-Scale Experiment and Energy Simulation. *Energies* **2019**, *12*, 1489. [\[CrossRef\]](#)
14. Nied, A.; Oliveira, J.; Stival, L.H.R.C.; Polli, H.B. Improving Washing Machine Performance Using Single-Phase Induction Motor Field-Oriented Control. In Proceedings of the IECON 2013—39th Annual Conference of the IEEE Industrial Electronics Society, Vienna, Austria, 10–13 November 2013; pp. 2917–2922. [\[CrossRef\]](#)
15. Correa, M.B.R.; Jacobina, C.B.; Lima, A.M.N.; Silva, E.R.C. A Three-Leg Voltage Source Inverter for Two-Phase AC Motor Drive Systems. In Proceedings of the 2001 IEEE 32nd Annual Power Electronics Specialists Conference (IEEE Cat. No. 01CH37230), Vancouver, BC, Canada, 17–21 June 2001; Volume 3, pp. 1458–1463. [\[CrossRef\]](#)
16. Jacobina, C.B.; Correa, M.B.R. Induction Motor Drive System for Low Power Applications. *IEEE Trans. Ind. Appl.* **1999**, *35*, 52–61. [\[CrossRef\]](#)
17. Chuan-Sheng, L.; Jonq-Chin, H.; Po-Cheng, C. Improvement of Driver Efficiency for the Single-Phase Motor. In Proceedings of the 2012 IEEE International Symposium on Industrial Electronics, Hangzhou, China, 28–31 May 2012; pp. 664–667. [\[CrossRef\]](#)
18. Correa, M.B.R.; Jacobina, C.B.; Lima, A.M.N.; Silva, E.R.C. Rotor-flux-oriented control of a single-phase induction motor drive. *IEEE Trans. Ind. Electron.* **2000**, *47*, 832–841. [\[CrossRef\]](#)
19. Dragotto, E. *Cost-Benefit Analysis of a Refrigerator Replacement Program for Low-Income Households in Brazil*; United States Agency for International Development: Washington, DC, USA, 2007; p. 38.
20. Byrne, D.M.; Oliner, S.D.; Sichel, D.E. How Fast Are Semiconductor Prices Falling? In *Finance and Economics Discussion Series (FEDS)*; Board of Governors of the Federal Reserve System: Washington, DC, USA, 2017. [\[CrossRef\]](#)
21. Waide, P.; Brunner, C.U. *Energy-Efficiency Policy Opportunities for Electric Motor-Driven Systems*; OECD Publishing: Paris, France, 2011. [\[CrossRef\]](#)
22. Boldea, I.; Nasar, S.A. *The Induction Machines Design Handbook*, 2nd ed.; The Electric Power Engineering Series; CRC Press/Taylor & Francis: Boca Raton, FL, USA, 2010.
23. Doncker, R.W.; Pulle, D.W.J.; Veltman, A. *Advanced Electrical Drives: Analysis, Modeling, Control*; Power Systems; Springer: Dordrecht, The Netherlands; Heidelberg, Germany, 2011. [\[CrossRef\]](#)
24. Zahedi, B.; Vaez-Zadeh, S. Efficiency Optimization Control of Single-Phase Induction Motor Drives. *IEEE Trans. Power Electron.* **2009**, *24*, 1062–1070. [\[CrossRef\]](#)
25. Jang, D.h. PWM Methods for Two-Phase Inverters. *IEEE Ind. Appl. Mag.* **2007**, *13*, 50–61. [\[CrossRef\]](#)
26. Kumsuwan, Y.; Premrudeepreechacharn, S.; Kinnares, V. A Carrier-Based Unbalanced PWM Method for Four-Leg Voltage Source Inverter Fed Unsymmetrical Two-Phase Induction Motor. *IEEE Trans. Ind. Electron.* **2013**, *60*, 2031–2041. [\[CrossRef\]](#)
27. Kumar, B.; Srinivas, S. Space Vector Based PWM of Dual Full-Bridge VSI Fed Two-Phase Induction Motor Drive. In Proceedings of the 2014 IEEE 23rd International Symposium on Industrial Electronics (ISIE), Istanbul, Turkey, 1–4 June 2014; pp. 667–672. [\[CrossRef\]](#)
28. Kumar, B.; Srinivas, S. Elliptical Space Vector PWM for Dual H-bridge VSI Fed Two-Phase Induction Motor Drive. In Proceedings of the 2016 IEEE International Conference on Power Electronics, Drives and Energy Systems (PEDES), Trivandrum, India, 14–17 December 2016; pp. 1–5. [\[CrossRef\]](#)
29. Konarik, R.; Pridala, M.; Jarabicova, M.; Sedo, J.; Laskody, T. Topologies of Converters for Two-Phase AC Motors. In Proceedings of the 2017 18th International Scientific Conference on Electric Power Engineering (EPE), Kouty nad Desnou, Czech Republic, 17–19 May 2017; pp. 1–6. [\[CrossRef\]](#)

30. Meshram, S.M.; Fadnis, A.Y. Direct Torque Control of Three-Leg Inverter Driving Two-Phase Induction Motor. In Proceedings of the 2015 IEEE Power, Communication and Information Technology Conference (PCITC), Bhubaneswar, India, 15–17 October 2015; pp. 242–247. [[CrossRef](#)]
31. Piyarat, W.; Hothongkham, P.; Charumit, C.; Kinnares, V. Simple Speed Control of an Asymmetrical Type Two-Phase Induction Motor Drive. In Proceedings of the ECTI-CON2010: The 2010 ECTI International Conference on Electrical Engineering/Electronics, Computer, Telecommunications and Information Technology, Chiang Mai, Thailand, 19–21 May 2010; p. 5.
32. Gupta, R. A Study of AC/DC Converter with Improved Power Factor and Low Harmonic Distortion. *Int. J. Comput. Sci. Eng.* **2012**, *4*, 1017–1029.
33. Lazaro, A.; Barrado, A.; Pleite, J.; Vazquez, R.; Vazquez, J.; Olias, E. Size and Cost Reduction of the Storage Capacitor in AC/DC Converters under Hold-up Time Requirements. In Proceedings of the IEEE 34th Annual Conference on Power Electronics Specialist, 2003. PESC '03, Acapulco, Mexico, 15–19 June 2003; Volume 4, pp. 1959–1964. [[CrossRef](#)]
34. Freescale Semiconductor. *Thermal Analysis of Semiconductors Systems*; White Paper; Freescale Semiconductor: Austin, TX, USA, 2008.
35. Künzi, R. Thermal Design of Power Electronic Circuits. In Proceedings of the 2014 CAS - CERN Accelerator School: Power Converters, Baden, Switzerland, 7–14 May 2014. [[CrossRef](#)]
36. Wintrich, A.; Nicolai, U.; Tursky, W.; Reimann, T. *Application Manual Power Semiconductors*, 2nd ed.; ISLE Verlag: Ilmenau, Germany, 2015.
37. Correa, M.; Jacobina, C.; Silva, E.; Lima, A. Vector control strategies for single-phase induction motor drive systems. *IEEE Trans. Ind. Electron.* **2004**, *51*, 1073–1080. [[CrossRef](#)]
38. Busatto, T.; Rönnberg, S.K.; Bollen, M.H.J. Comparison of Models of Single-Phase Diode Bridge Rectifiers for Their Use in Harmonic Studies with Many Devices. *Energies* **2021**, *15*, 66. [[CrossRef](#)]

Disclaimer/Publisher's Note: The statements, opinions and data contained in all publications are solely those of the individual author(s) and contributor(s) and not of MDPI and/or the editor(s). MDPI and/or the editor(s) disclaim responsibility for any injury to people or property resulting from any ideas, methods, instructions or products referred to in the content.